ChemComm

Accepted Manuscript

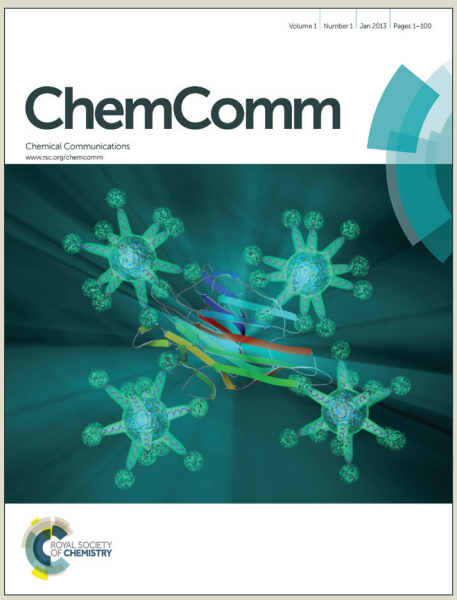

ROYAL SOCIETY OF CHEMISTRY

www.rsc.org/chemcomm

Cite this: DOI: 10.1039/c0xx00000x

www.rsc.org/xxxxxx

COMMUNICATION TYPE

A novel anode material derived from organic-coated ZIF-8 nanocomposites with high performance in lithium ion battery

Yuzhen Han, ‡[a] Pengfei Qi, ‡[a] Siwu Li,[a] Xiao Feng,[a] Junwen Zhou,[b] Haiwei Li,[a] Shuangyue Su,[a] Xingguo Li,[b] and Bo Wang*[,a]

Received (in XXX, XXX) Xth XXXXXXXXX 20XX, Accepted Xth XXXXXXXXX 20XX
DOI: 10.1039/b000000x

A general method of preparing nanocomposites from a metal-organic framework coated with hydroxyl, pyrrolyl and/or carboxyl functionalized organics is introduced. Pyrolysis of these nanocomposites gives anode materials with improved discharging capacity (750 mA h g^{-1}) and cyclability. They also show enhanced Coulombic efficiency of the initial 5-10 cycles and decreased internal impedance.

Lithium ion batteries (LIBs), as clean and convenient rechargeable batteries, are expected to continue playing important roles in energy storage.[1] To date, many efforts have been devoted to the research of anode materials with superior performance in LIBs applications. Graphite as a commercial anode material possesses the advantages of high Coulombic efficiency and impressive cycle stability, but suffers from its low theoretical capacity of 372 mA h g^{-1} and limited rate capability. Metal or metal oxides with higher energy density are desired candidate for anode materials. However, it still undergoes an undesirable large volume change, which leads to a dramatic falloff in capacity during cycling. Therefore, a raising interest is focused on developing alternative anode materials with higher reversible capacity to meet the requirement for energy storage for LIBs.[2-4]

Metal-organic frameworks (MOFs) are micro-porous materials synthesized by assembling metal ions with organic ligands. A lot of efforts during the past several years have been concentrated on preparing new MOF structures and exploiting their applications, including gas storage and separation, catalysis, sensing and drug delivery.[5] MOFs are regarded as attractive candidates for lithium ion electrode materials due to their host architectures that allow rapid insertions of species. Recently, several MOFs, such as MOF-5[6], MOF-199[7] and MIL-88[8], have been applied. However, either the limited capacity or the stability of the anode material in the first several circles was not satisfactory. One of the concerns of using MOFs or MOF-based materials for LIBs is indeed its extremely high surface area and predominant micro-pores. This may hamper the performance of MOFs resulting from low electronic conductivity and severe irreversible lithium storage. High surface area and predominant micro-pores might lead to more side reactions such as reductive decomposition of the electrolyte and formation of a solid electrolyte interface (SEI) layer.[9, 10] Moreover, these MOFs have low packing density and poor interparticle contacts lowering their volumetric energy density.[11] Therefore, pursuing of new MOF-based materials with moderate pore surface area and proper pore size distribution are crucial for improving their performance as anode materials. Pyrolyzing MOFs can effectively reduce their surface areas, expand their pores to mesopores and boost their conductivity. More importantly, given the right conditions, pyrolysis can still maintain the open diffusion channels and ensure the mono-dispersion of metal centers upon carbonization of the organic links in MOF backbone. For instance, after pyrolyzing, the Brunauer-Emmet-Teller (BET) surface area of MOF-5 drops from 3800 to 513 m^2 g^{-1}, and the average pore size increases from 1 to 35 nm.[6, 12] Nevertheless, this BET surface area is still too high to achieve ideal performance and indeed the low Coulombic efficiency and irreversible Li storage over the first 10 cycles are evident in the case of pyrolyzed MOF-5.[6] Compared with MOF-5, ZIF-8 nanocrystals with a lower surface area of 1700 m^2 g^{-1} and higher metal density (number of zinc clusters per volume, 2.4 nm^{-3} vs. 2.1 nm^{-3}) in the framework[13], (Fig. 1a) enabling the generation of more active metal centres after carbonization.[14] Moreover, lower specific surface area of the materials can reduce the initial irreversible capacities.

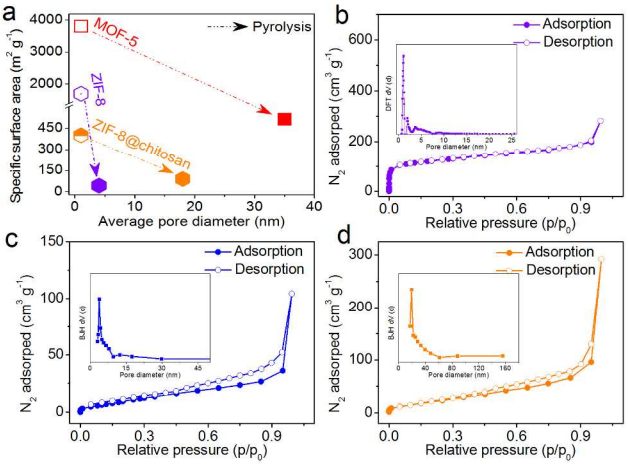

Fig. 1 (a) BET specific surface areas and average pore size of MOF-5, ZIF-8 and ZIF-8@chitosan before and after pyrolysis. (b-d) Nitrogen adsorption isotherms at 77 K, for (b) ZIF-8@chitosan, (c) ZIF-8-800N and (d) ZIF-8@chitosan-800N (e.g., "800N" denotes a sample heated at 800 °C under inert atmosphere.). Insets show the pore size distribution from BJH calculation based on the desorption branch of corresponding isotherm.

We herein introduce a general method of preparing anode active materials from series of nanocomposites that are derived from a metal-organic framework coated with hydroxyl, pyrrolyl and/or carboxyl functionalized organic compounds. Specifically, ZIF-8 nanoparticals coated with chitosan, glucose, citric, pyrrole, and β-cyclodextrin were prepared using mechanochemical synthetic approach. Then they were further pyrolyzed at 800 °C, at which temperature ZIF-8 frameworks were carbonized and most of the zinc ions can be retained. (ESI Fig. S1, the TGA of the mechanochemically synthesized ZIF-8 nanocrystals; the detailed experimental procedures can be found in the ESI and the schematic diagram is showed in Scheme 1)

Carbonization temperature of MOFs, as reported by other groups,[6, 15] is an important parameter to obtain desired carbon materials. Therefore we carbonized ZIF-8 at various temperatures (700, 800 and 900 °C). Although the obtained capacity of ZIF-8-800N is the highest compared with the materials pyrolyzed at 700 and 900 °C (Fig. S2), it is still impeded by rapid capacity fade, so the coating is necessary.

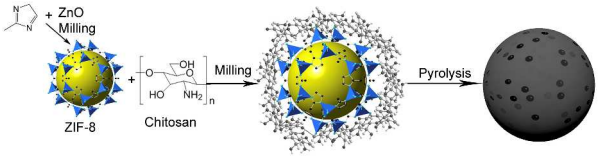

Scheme 1. Synthetic route of ZIF-8@chitosn-800N

These materials had been fully characterized by PXRD, FT-IR, SEM, TEM, Raman, XPS, and nitrogen adsorption measurements. Electrochemical performances of the materials after carbonization were tested and anode was prepared using these composites. Clearly, pyrolysis of thus-obtained nanocomposites has led to active anode materials with improved discharging capacity and cyclability in lithium ion battery. Especially the one derived from chitosan coated ZIF-8 nanocrystals (denoted as ZIF-8@chitosan) gives specific capacity at 750 mA h g^{-1} (calculated by active material) over 50 cycles and no apparent fading is shown. Extended long cycle test was further performed under 200 mA g^{-1} and the anode shows sexceptional stability over 300 cycles (Fig. S3, ESI). By virtue of the organic compounds that are introduced, these anode materials show enhanced Coulombic efficiency of the initial cycles and decreased internal impedance.

Powder X-ray diffraction (PXRD) patterns of the mechanochemically synthesized ZIF-8 and ZIF-8@chitosan are in agreement with the simulated pattern of ZIF-8 (Fig. S4). After pyrolyzing, only a broad peak at 2θ = 25° is observed for the sample derived from ZIF-8@chitosan (denoted as ZIF-8@chitosan-800N), indicating the amorphous nature of this carbon composite[16]. Scanning electron microscopy (SEM) and transmission electron microscopy (TEM) images of ZIF-8, ZIF-8@chitosan, ZIF-8-800N (direct pyrolysis of ZIF-8) and ZIF-8@chitosan-800N are shown in Fig. S5 and Fig. 2. The mechanochemically synthesized ZIF-8 crystals are homogeneous nanoparticles with average diameter of about 200 nm. The morphologies of nanoparticles become irregular for ZIF-8@chitosan (SEM, Fig. 2b) and TEM show the surface of ZIF-8 is coated by chitosan (Fig. S5a). According to the FT-IR, the absorptions caused by the stretching and vibrations of free –OH and $–NH_2$ on chitosan are largely reduced when grinding with ZIF-8, indicating strong interactions of these functional groups with zinc ions on the surface of ZIF-8 (Fig. S6). After pyrolysis, the particle sizes of these two materials are both altered into broader distributions. An agglomeration is occurred for ZIF-8-800N and ZIF-8@chitosan-800N (Fig. S5b and Fig. 2c). The elemental mappings on ZIF-8-800N and ZIF-8@chitosan-800N are shown in Fig. S7 and Fig. 2d, zinc ions are evenly distributed across both sample particles. Thus we could conclude that the mono-dispersion of Zn ions is mainly formed during the carbonization process of the framework and extra carbon source from the coating organics has little impact on the dispersion of ZnO particles. X-ray photoelectron spectroscopy (XPS) reveals the existence of Zn-O bonding, C-C bonding and slight amount of oxygen-functionalized carbon bonding[6] in ZIF-8@chitosan-800N (Fig. S8). XPS and PXRD results suggest that ZIF-8@chitosan-800N is composed of amorphous ZnO embedded in porous carbon-based scaffold.

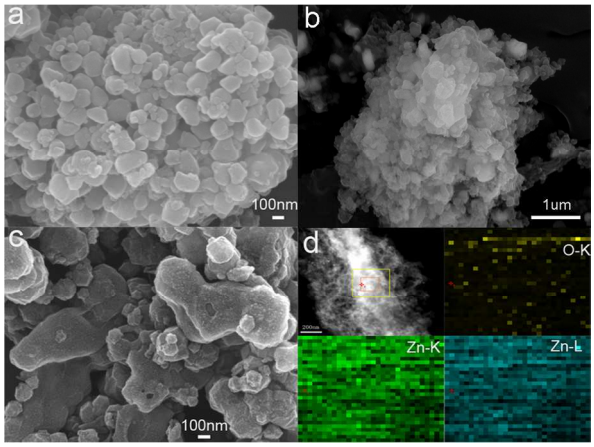

Fig. 2 (a) SEM image of ZIF-8 nanocrystals, (b) SEM image of ZIF-8@chitosan, (c) SEM image of ZIF-8@chitosan-800N, (d) TEM image and the elemental mappings of ZIF-8@chitosan-800N

To gain insight into the porous structures of these materials, nitrogen adsorption isotherms at 77 K were measured, after heating the sample under vacuum at 150 ºC for 6 h. This study reveals that the surface area of ZIF-8@chitosan is 400 m^2 g^{-1} which shows a sharp decrease comparing to that of ZIF-8. (Fig. 1b) After pyrolysis, ZIF-8-800N and ZIF-8@chitosan-800N possess lower surface areas of 44 m^2 g^{-1} and 90 m^2 g^{-1}, respectively. The rough surface texture and hierarchal nanostructures of both samples (Fig. S5b and Fig. 2c) are presumably caused by the carbonization of the organic links and partial collapse of the backbone as further determined by the thermal gravimetric analysis (Fig. S1). After pyrrolyzing samples in N_2, both isotherms show typical type IV curves with hysteresis hoops, indicating the mesoporous features (Fig. 1c and d). The pore volume of the ZIF-8-800N and ZIF-8@chitosan-800N samples are 0.16 cm^3 g^{-1} and 0.45 cm^3 g^{-1}, respectively. Pore size distribution calculated from the desorption isotherm using the Barrett-Joyner-Halenda (BJH) method (inset of Fig. 1c and d) indicates the presence of mesopores with an average pore diameter of 4 nm and 19 nm. Such mesopores are believed to be beneficial for accommodating the volume variations and facilitating the lithium ion transfer during the charge/discharge

cycling. [17-19] This low specific surface area correlates with the grain growth, particle aggregation and reduced porosity, which agrees with the data obtained by SEM and analyses. Investigation on the materials was performed by Raman spectroscopy. Fig. S9 shows the Raman spectra of the materials, exhibiting D and G bands centered at 1350 cm^{-1} and 1560 cm^{-1}, respectively. The relative ratios of the G band to the D band (I_G/I_D) were almost constant ($I_G/I_D \approx 1$). However an extra peak centered at 1460 cm^{-1} is evident in both ZIF-700N and ZIF-800N, which matches the absorption of the C-H[20] (Raman spectra of ZIF-8). These results supported the conclusion that carbonization at 800 ˚C can effectively enhance the graphitization of ZIF-8 while maintaining electrical active zinc ions.

Applying ZIF-8@chitosan-800N as the anode materials in LIBs exhibits outstanding charge/discharge efficiency and capacity retention (Fig. 3). It delivers a reversible capacity of 750 mA h g^{-1} at current density of 50 mA g^{-1}, and kept the capacity of 739 mA h g^{-1} after 50 cycles with a capacity retention of 99.6%. This result, as indicated in Fig. 3a, is dramatically improved comparing to that of ZIF-8-800N material. The irreversible capacity loss in the first two cycles is owing to the formation of solid electrolyte interphase (SEI).[21] For the subsequent cycle-life performance, the Coulombic efficiency appears to level off immediately and remains constant at 97%. It is showing that the SEI layer formed in the first time is fairly stable.

From the galvanostatic charge/discharge curve shown in Fig. 3b, we can find that most of the discharge capacity is below 1.0 V. It is effective and significant for the practical application for larger potential difference and power density. It also can be seen through the cyclic voltammetry profile (Fig. S10). In addition, the impedance associated with the charge-transfer resistance in ZIF-8@chitosan-800N (Fig. 3c) is lower than that of the commercial ZnO and ZIF-8-800N, demonstrating the excellent conductive capability of the rechargeable battery. [22, 23]

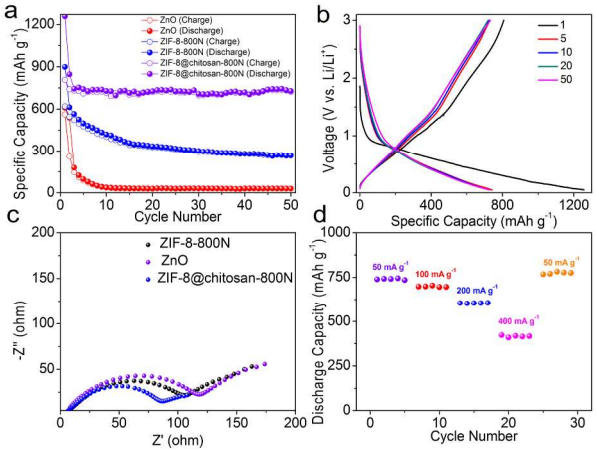

Fig. 3 (a) Cycle-life performances of ZnO, ZIF-8-800N, ZIF-8@chitosan-800N at current density of 50 mA g^{-1}. (b) Voltage profile of ZIF-8@chitosan-800N. (c) Nyquist plots for ZIF-8@chitosan-800N, commercial ZnO and ZIF-8-800N after four cycles. (d) Discharge capacity of ZIF-8@chitosan-800N at various current densities. The cells were cycled 50 times at a current density of 50 mA g^{-1} prior to variation of the current density from 50 to 800 mA g^{-1}.

To further examine the cycling stability and rate capacity of the cell, the discharge and charge cycles were further performed at various current densities (Fig. 3d). It is found that, the discharge capacity remains at 750, 700, 600 and 420 mA h g^{-1} at rates of 50, 100, 200 and 400 mA g^{-1}, respectively. (galvanostatic charge/discharge curve shown in Fig. S11) After enduring various charge-discharge rates, the electrode resumes its capacity of about 750 mA h g^{-1} with the rate back to 50 mA h g^{-1} and maintains this value without any apparent decay. The slight increase of the discharge capacity may attribute to part of the lithium ion remaining in the electrodes during charging with larger current densities.[24]

The theoretical specific capacity of ZnO is 978 mA h g^{-1}, while that of graphite is 372 mA h g^{-1}. The weight content of Zn and ZnO is 29.5% and 36.8%, respectively, calculated from elemental analysis by ICP (Inductive Coupled Plasma Emission Spectrometer) measurement. The active components in ZIF-8@chitosan-800N can be regarded as ZnO and nitrogen-doped graphite. It is believed that N-doped carbon materials[15, 25] as the active species in the anode of lithium ion battery[26] show improved electrochemical performance. The theoretical capacity will be estimated to be 549 mA h g^{-1} if we simply add the capacities according to their individual weight contributions. As mentioned above, the specific capacity of ZIF-8@chitosan-800N electrode can achieve 750 mA h g^{-1}, which is much higher than the calculated value. It is probably due to the uniformly distribution of ZnO in the porous carbon-based electrodes, derived from the original ZIF-8 architectures. It is further proved by Energy Dispersive X-Ray Spectroscopy (EDX) measurement that allows the estimation of the elemental content in the surface domains with the depth about 1 μm. The weight percent of Zn is found to be 24% (Fig. S12) which is consistent with the result from the ICP analysis. However, the XPS result shows the weight percentage of Zn at surface is 11%, much lower than the whole Zn weight. The reason is that we coated chitosan at the surface of ZIF-8 before pyrolysis, and the XPS measurement that allows the estimation of the elemental content in the surface domains with the depth about 10 nm. The uniformly distributed ZnO is beneficial for storing more lithium ion in the anodes, and thus leads to high specific capacities and better retention.

Besides chitosan, other biological compounds (*i.e.*, glucose citric, pyrrole, and β-cyclodextrin) were also utilized to coat ZIF-8 materials (PXRD is showed in Fig S4b). Through the nitrogen adsorption isotherms at 77 K of the samples coated by different compounds as showed in Fig. S13 and Fig. S14, we can find all the surface areas of the samples are lower than that of pure ZIF-8, and after pyrolysis a sharp decrease is occurred except for ZIF-8@citric. The pore size distribution of ZIF-8@glucose, ZIF-8@pyrrole, and ZIF-8@β-cyclodextrin is similar with that of ZIF-8, while ZIF-8@citric has a relatively broader pore size distribution as the ZIF-8 framework is partially undermined by mixing with the citric acid (Fig. S4b). After carbonization, these organic-coated materials show more mesopores similar as in the case of ZIF-8-800N. Importantly chitosan-coated carbonized sample, ZIF-8@chitosan-800N, yielded bigger pores around 19 nm whereas all the other samples only show pores smaller than 5 nm. This hierarchal pore structure of ZIF-8@chitosan-800N is critical in obtaining better electrochemical performance. These observations are in line with our previous discussion (Fig. 1).

We also carefully measured the anodic performance of all the

other organic-coated samples. Samples that are coated by glucose and citric show slight improvement over the sample derived from pure ZIF-8, that is, the capacity still drops dramatically from 800 to 300 mA h g^{-1} over 50 and 30 cycles (Fig. S15a and b). Pyrrole and β-cyclodextrin-coated samples, on the other hand, have better performance than carbonized pristine ZIF-8 and their capacity fell down to 400 mA h g^{-1} after 50 cycles (Fig. S15c and d).

In summary, we have demonstrated an effective mechanochemical route to the synthesis of ZIF-8 nanocrystals and ZIF-8@chitosan for battery applications. Chitosan, as a simple biomolecule, is environmental friendly and readily available. A novel lithium ion battery anode material is synthesized by pyrolyzing ZIF-8@chitosan nanocomposite and shows high specific capacity, lower impedance and impressive cycling stability. By virtue of the general and facile synthetic approach and outstanding electrochemical performance, this work may shed light on the future research in preparation of anode materials with enhanced performance through biomolecule-coated MOFs or ZIFs for practical energy applications.

This work was financially supported by the 973 Program 2013CB834704; "1000 Plan (Youth)"; the National Natural Science Foundation of China (Grant No. 21201018; 21231002; 21173021; 21276026).

Notes and references

[a] *Key Laboratory of Cluster Science, Ministry of Education of China, School of Chemistry, Beijing Institute of Technology, 5 South Zhongguancun Street, Beijing, 100081, P.R. China.*
E-mail: bowang@bit.edu.cn.
[b] *College of Chemistry and Molecular Engineering, Peking University, 5 Yiheyuan Road, Beijing, 100871, P.R. China.*

† Electronic Supplementary Information (ESI) available: Synthetic materials and instruments, synthetic methods, and experimental are included in the supporting information. See DOI: 10.1039/b000000x/

‡ These authors contributed equally to this work.

1. J. M. Tarascon and M. Armand, *Nature*, 2001, **414**, 359-367.
2. A. Magasinski, P. Dixon, B. Hertzberg, A. Kvit, J. Ayala and G. Yushin, *Nat. Mater.*, 2010, **9**, 353-358.
3. F. Cheng, J. Liang, Z. Tao and J. Chen, *Adv. Mater.*, 2011, **23**, 1695-1715.
4. B. Scrosati, J. Hassoun and Y. K. Sun, *Energ. Environ. Sci.*, 2011, **4**, 3287-3295.
5. H. Furukawa, K. E. Cordova, M. O'Keeffe and O. M. Yaghi, *Science*, 2013, **341**, DOI:10.1126/science.1230444.
6. S. J. Yang, S. Nam, T. Kim, J. H. Im, H. Jung, J. H. Kang, S. Wi, B. Park and C. R. Park, *J. Am. Chem. Soc.*, 2013, **135**, 7394-7397.
7. R. B. Wu, X. K. Qian, F. Yu, H. Liu, K. Zhou, J. Wei and Y. Z. Huang, *J. Mater. Chem. A*, 2013, **1**, 11126-11129.
8. X. Xu, R. Cao, S. Jeong and J. Cho, *Nano Lett.*, 2012, **12**, 4988-4991.
9. C. C. Liang, D. F. Cheng, S. J. Ding, P. F. Zhao, M. S. Zhao, X. P. Song and F. Wang, *J. Power Sources*, 2014, **251**, 351-356.
10. S. L. Xiong, J. S. Chen, X. W. Lou and H. C. Zeng, *Adv. Funct. Mater.*, 2012, **22**, 861-871.
11. H. E. Wang, J. Jin, Y. Cai, J. M. Xu, D. S. Chen, X. F. Zheng, Z. Deng, Y. Li, I. Bello and B. L. Su, *J. Colloid. Interf. Sci.*, 2014, **417**, 144-151.
12. A. D. Steven S. Kaye, Omar M. Yaghi, and Jeffrey R. Long, *J. Am. Chem. Soc.*, 2007, **129**, 14176-14177.
13. K. S. Park, Z. Ni, A. P. Cote, J. Y. Choi, R. D. Huang, F. J. Uribe-Romo, H. K. Chae, M. O'Keeffe and O. M. Yaghi, *P. Natl. Acad. Sci. USA.*, 2006, **103**, 10186-10191.
14. D. Zhao, J. L. Shui, C. Chen, X. Q. Chen, B. M. Reprogle, D. P. Wang and D. J. Liu, *Chem. Sci.*, 2012, **3**, 3200-3205.
15. H. L. Jiang, B. Liu, Y. Q. Lan, K. Kuratani, T. Akita, H. Shioyama, F. Q. Zong and Q. Xu, *J. Am. Chem. Soc.*, 2011, **133**, 11854-11857.
16. L. Mao, K. Zhang, H. S. O. Chan and J. S. Wu, *J. Mater. Chem.*, 2012, **22**, 80-85.
17. P. Y. Li, J. C. Deng, Y. Li, W. Liang, K. Wang, L. T. Kang, S. Z. Zeng, S. H. Yin, Z. G. Zhao, X. G. Liu, Y. Z. Yang and F. Gao, *J. Alloy. Compd.*, 2014, **590**, 318-323.
18. Y. G. Guo, J. S. Hu and L. J. Wan, *Adv. Mater.*, 2008, **20**, 4384-4384.
19. D. Bresser, E. Paillard, R. Kloepsch, S. Krueger, M. Fiedler, R. Schmitz, D. Baither, M. Winter and S. Passerini, *Adv. Energy Mater.*, 2013, **3**, 513-523.
20. G. Kumari, K. Jayaramulu, T. K. Maji and C. Narayana, *J. Phys. Chem. A*, 2013, **117**, 11006-11012.
21. Z. S. Wu, W. C. Ren, L. Wen, L. B. Gao, J. P. Zhao, Z. P. Chen, G. M. Zhou, F. Li and H. M. Cheng, *Acs Nano*, 2010, **4**, 3187-3194.
22. J. Jamnik and J. Maier, *Phys. Chem. Chem. Phys.*, 2003, **5**, 5215-5220.
23. Y. Wu, Y. Wei, J. P. Wang, K. L. Jiang and S. S. Fan, *Nano Lett.*, 2013, **13**, 818-823.
24. R. G. Ma, Y. C. Dong, L. J. Xi, S. L. Yang, Z. G. Lu and C. Y. Chung, *Acs Appl. Mater. Inter.*, 2013, **5**, 892-897.
25. R. Li, X. Ren, X. Feng, X. Li, C. Hu and B. Wang, *Chem. Commun.*, 2014, **50**, 6894-6897.
26. Z. S. Wu, W. C. Ren, L. Xu, F. Li and H. M. Cheng, *Acs Nano*, 2011, **5**, 5463-5471.